MULTIGRID CALCULATIONS FOR CASCADES

Antony Jameson and Feng Liu
Princeton University, Princeton, NJ 08544

1. Introduction

Development of numerical methods for internal flows such as the flow in gas turbines or compressors has generally met with less success than that for external flows, due to the complexity of the flow pattern. Potential flow methods had been the major approach in cascade flow calculations until fairly recently, when solution of the Euler equations became practically feasible. The most widely used Euler method has been Denton's finite volume method [1].

Like all explicit methods, Denton's method suffers from the limit of the CFL condition. Implicit schemes have been developed to yield convergence in a smaller number of time steps. This will only pay, however, if the decrease in the number of time steps outweighs the increase in the computational effort per time step consequent upon the need to solve coupled equations. A review of various time stepping schemes is given by Jameson [2].

The finite volume method with a multiple stage time stepping scheme developed by Jameson [3] has been very successful in calculating external flows. This method has the advantage of separated spatial and time discretizations and is easy to implement. The finite–volume discretization applies directly in the physical domain and is in conservation form. Adaptive numerical dissipation of blended first and third differences in the same conservation from as the convection fluxes is used to provide the necessary higher order background dissipation, and also the dissipation for capturing shocks. Subramanian [4] and Holmes [5] have successfully extended the 4–stage Runge–Kutta scheme to cascade calculations.

Instead of the 4–stage scheme the present work uses a more flexible multistage scheme together with locally varying time steps, enthalpy damping and implicit residual averaging to extend the stability limit and accelerate convergence. Finally very rapid convergence is obtained by applying an effective multigrid method [6]. Since the necessary dissipation is added separately from the discretization of the conservation laws, the amount of dissipation can be carefully optimized to improve the accuracy. Two–dimensional subsonic, transonic and supersonic cascade flows have been calculated using this method. The results show excellent accuracy and convergence.

2. Numerical Method

With a cell centered finite volume scheme a system of ordinary differential equations is obtained by applying the integral form of the Euler equations separately to each cell

$$\frac{d}{dt}(S_{ij}W_{ij}) + Q_{ij} - D_{ij} = 0 \tag{1}$$

where S_{ij} is the cell area, W_{ij} is the flow variable (either mass, momentum or energy) defined at the center of the cell, Q_{ij} is the net flux out of the cell and D_{ij} is the artificial dissipation term. The dissipation term D_{ij} is a blending of fluxes of first and third order compared to the convection term Q_{ij}. The first order dissipation is switched off in a smooth region and on in the neighborhood of a shock by multiplying it with a pressure sensor

$$\gamma_{ij} = \frac{|P_{i+1,j} - 2P_{ij} + P_{i-1,j}|}{|P_{i+1,j} + 2P_{ij} + P_{i-1,j}|}$$

γ_{ij} is small in a smooth region and of order one across a shock. This sensor has proved to be very effective for transonic flow. For supersonic flow, however, it can produce large values in sharp expansion regions where first order dissipation is not needed. To eliminate this possibility an alternative sensor based on entropy increase can be used, since entropy increases across a shock but remains constant across expansion waves. This may be defined as

$$\gamma_{ij} = |S_{i+1/2,j} - S_{i-1/2,j}|$$

Another alternative is to try to detect compressions from the divergence of velocity. Accordingly one can set

$$\gamma_{ij} = \begin{cases} -\nabla\cdot\vec{q} & \text{if } \nabla\cdot\vec{q} < 0 \\ 0 & \text{if } \nabla\cdot\vec{q} > 0 \end{cases}$$

γ_{ij} is then proportional to $\nabla\cdot\vec{q}$ across shocks, which simulates physical viscous effects, and zero across expansion waves.

Equation (2) is integrated in time by an explicit multistage scheme. Multistage schemes are chosen because of their extended stability limit and high frequency damping properties which are appropriate for multigrid schemes. To increase the rate of convergence local time steps, enthalpy damping and implicit residual averaging techniques have been used. These techniques enable us to use Courant numbers up to almost 10. The most effective method of accelerating convergence, however, is the multigrid method. Auxiliary meshes are introduced by doubling the

mesh spacing. Values of the flow variables are transferred to a coarser grid by a rule that conserves mass, momentum and energy. The multistage scheme is reformulated as described in [6] with the result that the solution on a coarse grid is driven by the residuals collected on the next finer grid. The process is repeated on successively coarser grids. Finally the corrections are passed back to the next finer grid by bilinear interpolation. Both V–cycle and W–cycle strategies have been used.

3. Boundary Conditions

The scheme has been programmed for different mesh topologies. For cascade calculations we usually encounter four types of boundaries; wall, periodic, inlet and outlet. Care must be exercised in treating these boundaries since internal flow is more sensitive to the boundary conditions than external flow. Inconsistency may cause large numerical errors and instabilities.

For wall boundaries zero normal velocity is imposed, and we use the normal momentum equation to extrapolate the pressure to the wall. Equivalent flow variables are imposed on corresponding periodic boundaries. They are updated as interior points. Based on characteristic analysis the entropy, which is equivalent to specifying total pressure, total enthalpy and the flow angle are specified on the inlet flow boundary for subsonic flow. The other independent flow variable is extrapolated from the interior by using the Riemann invariant for a one–dimensional flow normal to the boundary. Let the total entropy, enthalpy and flow angle far upstream be S_∞, H_∞ and α_∞. These values are specified for the fictitious cells upstream of the computational domain. The one–dimensional Riemann invariant normal to the boundary is

$$Re = q_{ne} + \frac{2c_e}{\gamma-1}$$

where the subscript e indicates interior values, q_n is the normal velocity to the inflow boundary and c is the speed of sound. For supersonic flow, all variables are specified on the inlet boundary. Conversely on the outlet flow boundary,only the pressure is specified for subsonic flow, while the entropy and total enthalpy plus one Riemann invariant are extrapolated. If the pressure of the initial flow field is very different from the specified back pressure, it is necessary for stability to adjust the back pressure gradually from the initial value to the specified value for the first few time steps. For supersonic flow in the axial direction all flow variables are extrapolated.

4. Test Cases

A. NACA 0012 Cascade

The first test case is a cascade with unstaggered NACA 0012 profiles and with solidity 1. An O–mesh is generated by an elliptic generator. Both a subsonic and a transonic case have been calculated. Figure 1 shows the Mach contours obtained for the transonic case with inlet Mach number 0.7. The Mach number in front of the shock is about 1.3 in contrast to the subcritical flow for the isolated airfoil at the same upstream Mach number. Figure 2 shows the convergence history of our computation with a 4 level multigrid scheme for the same cascade at inlet Mach number 0.4. The computation is started from a uniform flow. The work unit in the figure is the actual work equivalent to the number of cycles of a single grid iteration. It includes the extra work for the multigrid scheme. Comparison with the convergence history for the same case of an implicit ADI scheme by Schäfer [7] shows that the present scheme has a much faster convergence rate. Figure 3 shows the convergence history for the transonic case. We can see that the fast convergence rate remains about the same for the transonic case.

B. Hobson's Impulse Cascade

One of the most difficult test cases for cascade calculations is the Hobson shock free impulse cascade. It has very thick airfoils and was designed by the hodograph method to give a shock free supersonic pocket. Since any such shock free solution is isolated in the sense that a small perturbation in the flow conditions or airfoil shape can cause a shock wave to occur, Hobson's cascade provides a difficult test of both the accuracy and convergence for any numerical method. Ives calculated the flow of this cascade by a potential flow method [8]. The result, however, showed an obvious shock terminating the supersonic pocket in both the Cp distribution and Mach number contour pictures. Figure 4 shows the Cp distribution obtained by the present method. It is essentially shock free and in close agreement with the original hodograph design. Figure 5 shows the Mach number contours of the same solution. The smooth symmetric pattern is another indication of the accuracy. The convergence history is shown in figure 6. Again it demonstrates the fast convergence rate of the method. The results shown here, we believe, are about the best as yet published. However, it must be pointed out that the original surface definition by the hodograph method is very coarse. It has only 39 points on the upper surface and 15 points on the lower surface. A refinement of the surface definition is needed for more accurate numerical comparisons.

C. Supersonic Wedge Cascade

Denton proposed a wedge cascade as a test case for capturing oblique shocks in cascades [1]. Figure 7 shows our solution for such a cascade with inlet Mach number 2. The shock reflected from the lower blade is designed to be exactly canceled out at the corner of the upper blade, giving a uniform flow between the parallel surfaces and an expansion off the downstream

corner. This design gives a good test case for numerical methods, since smearing may prevent complete cancellation of the reflected shock, and thus may produce a nonuniform region downstream. Figure 8 shows the distribution on the blade obtained by the present method. Comparison of our results with the analytic solution and that of [1] shows that the present method is of higher accuracy than Denton's. An interesting result is the prediction of two trailing edge shocks from each blade, which interact with shocks from other blades. The interaction of the shocks through the periodic boundaries was not shown in [1].

Despite the improvement over Denton's results, the reflected shock is not completely cancelled by the upper blade, and this causes oscillations in the Mach number distribution. Furthermore, the Mach number in the expansion region is lower than that of the analytic solution although the pressure has fully recovered to the analytic value as shown in Fig. 8. This is an indication of entropy production, and may have been caused by the first order dissipation in that region. Use of the alternative sensors based on entropy change or the divergence of velocity have shown improvements, but the problem remains.

D. VKI Turbine Cascade

Finally, the turbine cascade as proposed on a VKI workshop [9] is tested. Figure 10 shows the pressure contours of the solution. While the Cp distribution deviates from the experimental data near the trailing edges, the convergence shown in figure 11 is far better than any one of those reported in [9]. The deviation from experimental data, which is present in all solutions of the workshop, may be attributed to the blunt trailing edge of the blade since viscous effects can not be ignored there.

5. Conclusion

A finite volume method with a multistage time stepping scheme is used to calculate 2–dimensional cascade flow. The stability limit of the explicit scheme is extended by using implicit residual averaging. Convergence is accelerated by using locally varying time steps, enthalpy damping and most of all an effective multigrid method. Adaptive numerical dissipation is used for capturing shocks. Our results for the NACA 0012 cascade, the Hobson shock free cascade and the supersonic wedge cascade show excellent accuracy and convergence in comparison with the results by other investigators. To resolve the flow near the blunt trailing edge of a turbine cascade, however, it will be necessary to use a viscous flow model.

References

1. Denton, J.D., "A Improved Time Marching Method for Turbomachinery Flow Calculation", J. of Engineering for Gas Turbines and Power, Vol. 105, July 1983.

2. Jameson, A., "Successes and Challenges in Computational Aerodynamics", AIAA Paper 87–1184–CP, Honolulu, Hawaii, 1987.

3. Jameson, A., Schmidt, W., and Turkel, E., "Numerical Solutions of Euler Equations by Finite Volume Methods Using Runge–Kutta Time Stepping Schemes", AIAA Paper 81–1259, June 1981.

4. Subramanian, S.V. and Bozzola, R., "Computation of Transonic Flows in Turbomachines Using the Runge–Kutta Integration Scheme", AIAA J., Vol. 25, No. 1.

5. Holmes, D.G. and Tong, S.S., "A Three–Dimensional Euler Solver for Turbomachinery Blade Rows", J. of Engineering for Gas Turbines and Power, Vol. 107, April 1985.

6. Jameson, A., "Transonic Flow Calculations", MAE Report #1651, Princeton University, July 1983.

7. Schäfer, O., Frühauf, H.H., Bauer, B., and Guggolz, M., "Application of a Navier–Stokes Analysis to Flows through Plane Cascades", J. of Engineering for Gas Turbines and Power, Vol. 108, January 1986.

8. Ives, D.C. and Liutermoza, J.F., "Second–Order–Accurate Calculation of Transonic Flow Over Turbomachinery Cascades", AIAA J. Vol. 17, No. 8, 1979, p. 870.

9. "Numerical Methods for Flows in Turbomachinery Blading", Von Karman Institute for Fluid Dynamics Lecture Series 1982–05, Vol. 3, April 26–30, 1982.

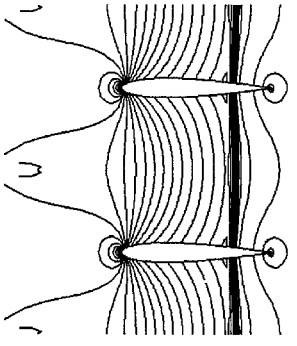

Fig. 1 Mach Number Contours for a NACA 0012
Cascade at M = 0.7, 161x33 Grid

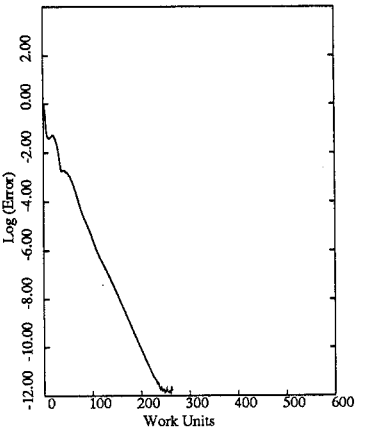

Fig. 2 Convergence History for a NACA 0012
Cascade at M = 0.4
Resid1 : 0.14e-01 Resid2 : 0.25e-13 Rate : 0.9027

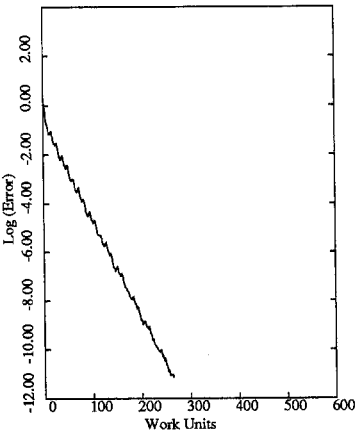

Fig. 3 Convergence History for a NACA 0012
Cascade at M = 0.7
Resid1 : 0.36e-01 Resid2 : 0.26e-12 Rate : 0.9075

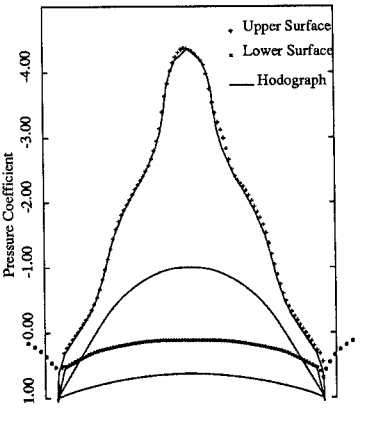

Fig. 4 Pressure Coefficient Distribution over Hobson's
Shock-Free Cascade

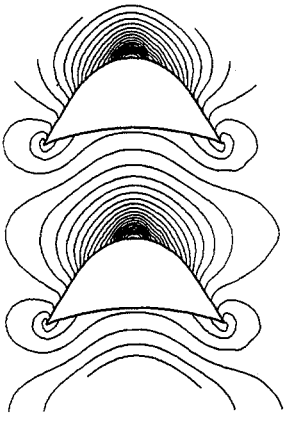

Fig. 5 Mach Contours of Hobson's Shock-Free Cascade
161x33 Grid

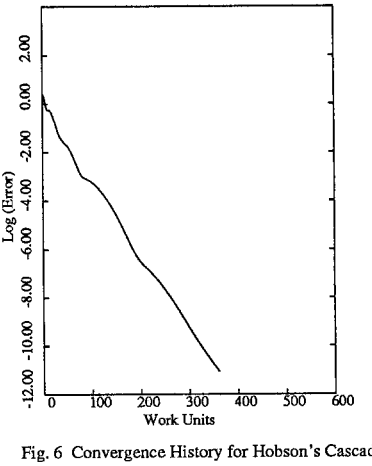

Fig. 6 Convergence History for Hobson's Cascade
Resid1 : 0.31e-01 Resid2 : 0.28e-12 Rate : 0.9319

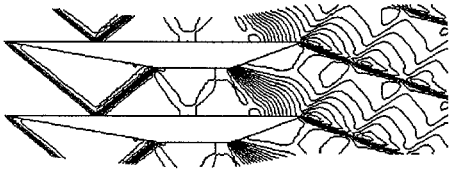

Fig. 7 Pressure Contours of a Wedge Cascade
M = 2. 161x33 Grid

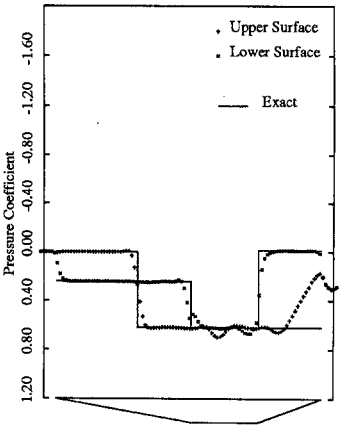

Fig. 8 Pressure Coefficient Distribution on a Wedge Cascade

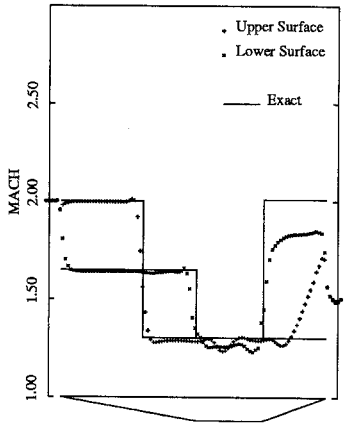

Fig. 9 Mach Number Distribution on a Wedge Cascade

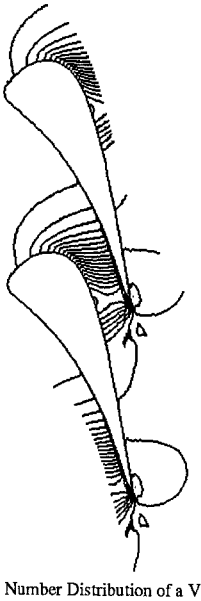

Fig. 10 Mach Number Distribution of a VKI Cascade
77x21 Grid

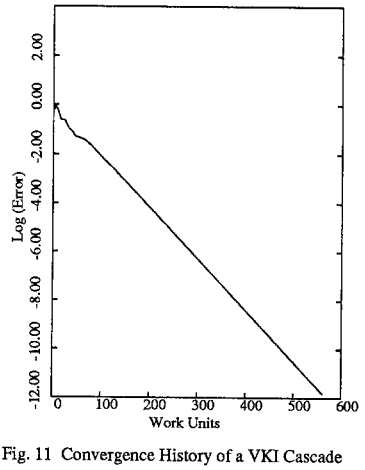

Fig. 11 Convergence History of a VKI Cascade
Resid1 : 0.66e+00 Resid2 : 0.99e-12 Rate : 0.9527